Atomic-Scale Multimodal Characterization of Self-Assembled InAs/InGaAlAs Quantum Dots

Yudai Yamaguchi,[†,] Yuta Inaba,[†] Ryoji Arai,[†] Yuya Kanitani,[†] Yoshihiro Kudo,[†] Michinori Shiomi,[†] Daiji Kasahara,[†] Mikihiro Yokozeki,[†] Noriyuki Fuutagawa,[†] Jun Uzuhashi,[‡] Tadakatsu Ohkubo,[‡] Kazuhiro Hono,[‡] Kouichi Akahane,[§] Naokatsu Yamamoto[§], and Shigetaka Tomiya[†]*

[†]Sony Semiconductor Solutions Corporation, Atsugi, Kanagawa 243-0014, Japan

[‡]National Institute for Materials Science, Tsukuba, Ibaraki 305-0047, Japan

[§]National Institute of Information and Communications Technology, Koganei, Tokyo 184-8795, Japan

Corresponding Author

***** Yudai Yamaguchi.

E-mail: Yudai.Yamaguchi@sony.com

ABSTRACT Self-assembled quantum dots (QDs) are potential candidates for photoelectric and photovoltaic devices because of their discrete energy levels. The characterization of QDs at the atomic level using a multimodal approach is crucial to improve device performance because QDs are nanostructures with highly correlated structural parameters. In this study, scanning transmission electron microscopy, geometric phase analysis, and atom probe tomography were

employed to characterize structural parameters such as the shape, strain, and composition of self-assembled InAs-QDs with InGaAlAs spacer layers. The measurements revealed characteristic AlAs-rich regions above the QDs and InAs-rich regions surrounding the QD columns, which can be explained by the relationship between the effect of strain and surface curvature around the QD. The methodology described in this study accelerates the development of future QD devices because its multiple perspectives reveal phenomena such as atomic-scale segregations and allow for more detailed discussions of the mechanisms of these phenomena.

TOC Graphic

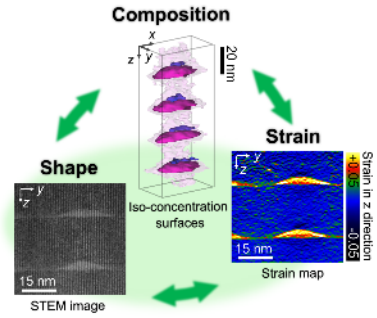

KEYWORDS quantum dot, atom probe tomography, transmission electron microscopy, geometric phase analysis, multimodal characterization

Self-assembled InAs quantum dots (QDs) have attracted considerable attention in various fields such as optoelectronics and photovoltaics because their band gap corresponds to the infrared region and discrete energy levels.[1–5] InAs-QDs are self-assembled *via* the Stranski–Krastanov (SK) mode growth, wherein a few atomic wetting layers of InAs are deposited on InP or GaAs substrates, driven by the strain energy.[6] Multistacking QDs can improve their performance; however, their crystal quality degrades because of the large strain.[7–9] Therefore, a strain-compensating structure that balances the macroscopic strain in the entire system using spacer layers with lattice strains in a direction opposite to that in InAs-QDs has been developed for achieving high-quality multistacked InAs-QDs.[10–13] InGaAlAs spacer layers are suitable for multistacking because they cancel the strain of InAs-QDs by changing the composition and prevent the segregation of In, thereby improving QD size uniformity.[14] The properties of QDs depend on structural parameters such as composition, shape, size, and strain, and these parameters must be understood and controlled to improve device performance.[15–19] QDs are nanostructures, and therefore, they require atomic-scale characterization. Further, the structural parameters of QDs are expected to be complexly correlated, and hence, multimodal characterization is required to understand the complete picture in detail. Although some structural parameters of QDs have been studied through various methods,[20–27] a multimodal characterization at atomic-scales, covering the shape, composition, and strain, are yet to be performed.

Scanning transmission electron microscopy (STEM) can characterize the nanostructure at the atomic level, and geometric phase analysis (GPA) can extract strain information from the STEM image.[28] These techniques are suitable for characterizing the QD nanostructure and strain.[20–23] Atom probe tomography (APT) is a three-dimensional (3D) composition-characterization technique with high spatial resolution in the sub-nanometer scale and a relatively low detection

limit, thereby rendering it best-suited for evaluating the elemental distributions around the QDs.[24–26] In this study, we combined these aforementioned techniques for characterizing structural parameters of multistacked self-assembled InAs-QDs with InGaAlAs spacer layers on an InP substrate. Subsequently, we identified atomic-scale segregations reflecting the shape and distribution of QDs, such as InAs-rich regions around the QD columns and AlAs-rich regions directly above QDs in the InGaAlAs spacer layer. The structural parameters of each QD were found to be highly interrelated: tensile and compressive strains were observed in the InAs-rich and AlAs-rich regions, respectively. Further, this characterization revealed the presence of Ga and Al atoms inside InAs-QDs due to diffusion from the InGaAlAs spacer layer. We characterized the distribution of In, Ga, and Al atoms inside InAs-QDs and observed that the distributions of these atoms were clearly correlated with each other.

The sample characterized in this study includes an InP(311)B substrate, an InP buffer layer, and a superlattice of 20-period self-assembled InAs-QD/$In_xGa_yAl_{1-x-y}As$ (x = 0.512, y = 0.212) spacer layer. The InP buffer and InGaAlAs spacer layers were 100 and 23 nm thick, respectively. The composition and thickness of the InGaAlAs layers were adjusted to compensate for the strain in the InAs-QDs in the system.[13]

Figures 1(a) and 1(b) present the cross-sectional high-angle annular dark-field STEM (HAADF-STEM) image observed in the [$\bar{2}33$] direction and its higher magnification image, respectively. QDs aligned in the direction of crystal growth and the sizes of all QDs in a column were approximately the same. Figure 1(a) show that the spacer layers between QDs in the same QD column exhibit brighter contrast than does the area without a QD column, forming a stripe-like bright contrast that includes the QD columns (e.g., the area enclosed by the white dashed line in the figure). The intensity profile of the HAADF-STEM image also reveals the presence of stripe-

like bright contrast (Figure S1). Dark contrast can be observed near the apex of each QD in Figure 1(b) (white arrows). Figure 1(c) presents the plan-view HAADF-STEM image observed from the [311] direction. The STEM image reveals information regarding the 3−4 layers of InAs-QD in the 80-nm-thick thin film specimen. The bright contrast in the figure corresponds to the positions of the QDs, indicating that QDs are elliptical in shape and their major axis is roughly parallel to the [$\bar{2}$33] direction. Figures 1(d) and 1(e) show the distributions of the major and minor axis lengths of the QDs observed in Figure 1(c), respectively. These results present variations in the sizes of the QDs. The high-magnification plan-view HAADF-STEM image in Figure 1(f) shows a dark streak-like contrast in the center of the QD, parallel to the major-axis (white arrow in the figure). However, a clear dark contrast was not observed for the small QDs (orange arrow in the figure). The dark contrast in the center of the QD is the same phenomenon as that observed at the QD apex in Figure 1(b).

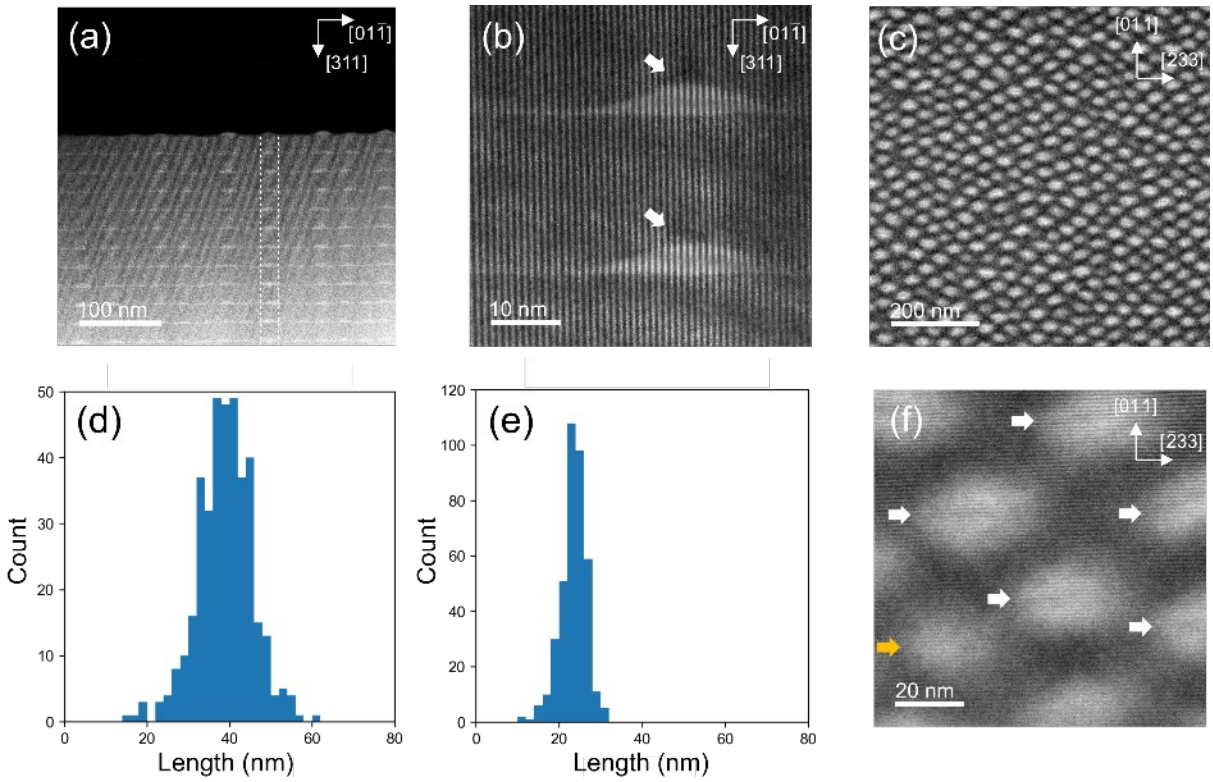

Figure 1. (a) Cross-sectional HAADF-STEM image observed from the [$\bar{2}33$] direction. (b) High-magnification HAADF-STEM image of (a). (c) Plan-view HAADF-STEM image observed from the [311] direction. Distributions of the (d) major-axis and (e) minor-axis lengths of the QDs observed in (c). (f) High-magnification plan-view HAADF-STEM image in (c).

Figures 2(a)–(d) present the high-magnification cross-sectional HAADF-STEM image observed from the [$\bar{2}33$] direction (different region from that in Figure 1(b)) and the strain maps (e_{zz}, e_{yy}, and e_{yz}) calculated by GPA, respectively. The spacer layer below the QD on the substrate side is used as the reference region for strain calculation, as demonstrated by the white box in Figure 2(a); each strain map indicates the relative strain (lattice expansion and compression). Strain calculations were performed using the (311) and ($0\bar{2}2$) diffraction points. Figure 2(a) shows a dark contrast near the apex of the QD (white arrows in the figure), which is similar to that in Figure 1(b). Figure 2(b) depicts the compressive strain in the region directly above the QD (white arrows in the figure). The stronger tensile strain at the QD interface is caused by the geometry of the QD, as is evident from the previous strain calculations of InAs-QDs.[22] Figure 2(c) shows that the stripe-like region in QD columns has a more expanded lattice than the other regions. Figure 2(d) shows the pairs of shear strains in opposite directions along the left and right sides of the QD surface.

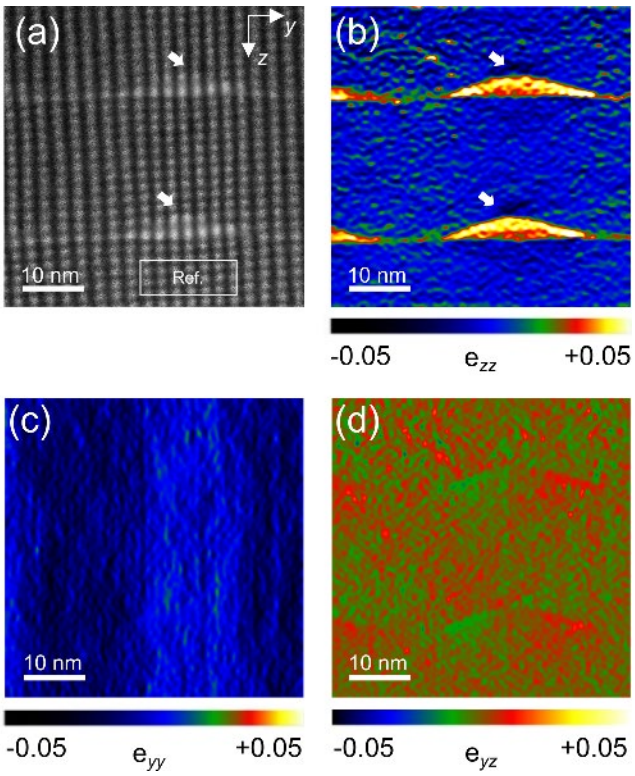

Figure 2. (a) High-magnification cross-sectional HAADF-STEM image observed from the [$\bar{2}$33] direction (different region from the view in Figure 1(b)). The reference region for the strain calculation is indicated by the white frame. (b) Normal strain (e_{zz}) map in the *z*-direction, (c) normal strain map in the *y*-direction (e_{yy}), and (d) shear strain (e_{yz}) map calculated from (a).

Figure 3(a) presents the 3D distributions of the InAs-QDs obtained from APT. The InAs-QDs are presented by iso-concentration surfaces[29] with an In concentration ([In counts]/[Al counts + Ga counts + In counts]) of 70%. Figures 3(b) and 3(c) illustrate a QD column containing QDs with an in-plane sizes of ~32 nm × 20 nm (blue frame in Figure 3(a)) and ~24 nm × 16 nm (green frame in Figure 3(a)), respectively. The iso-concentration surfaces of 33% Al, 57% In, and 70% In are indicated in blue, translucent pink, and pink, respectively. The QDs shown in Figures 3(b) and 3(c) are labeled QD-A–D and QD-a–d, respectively, from the surface side. Each QD in a column is aligned vertically and has an almost uniform size.

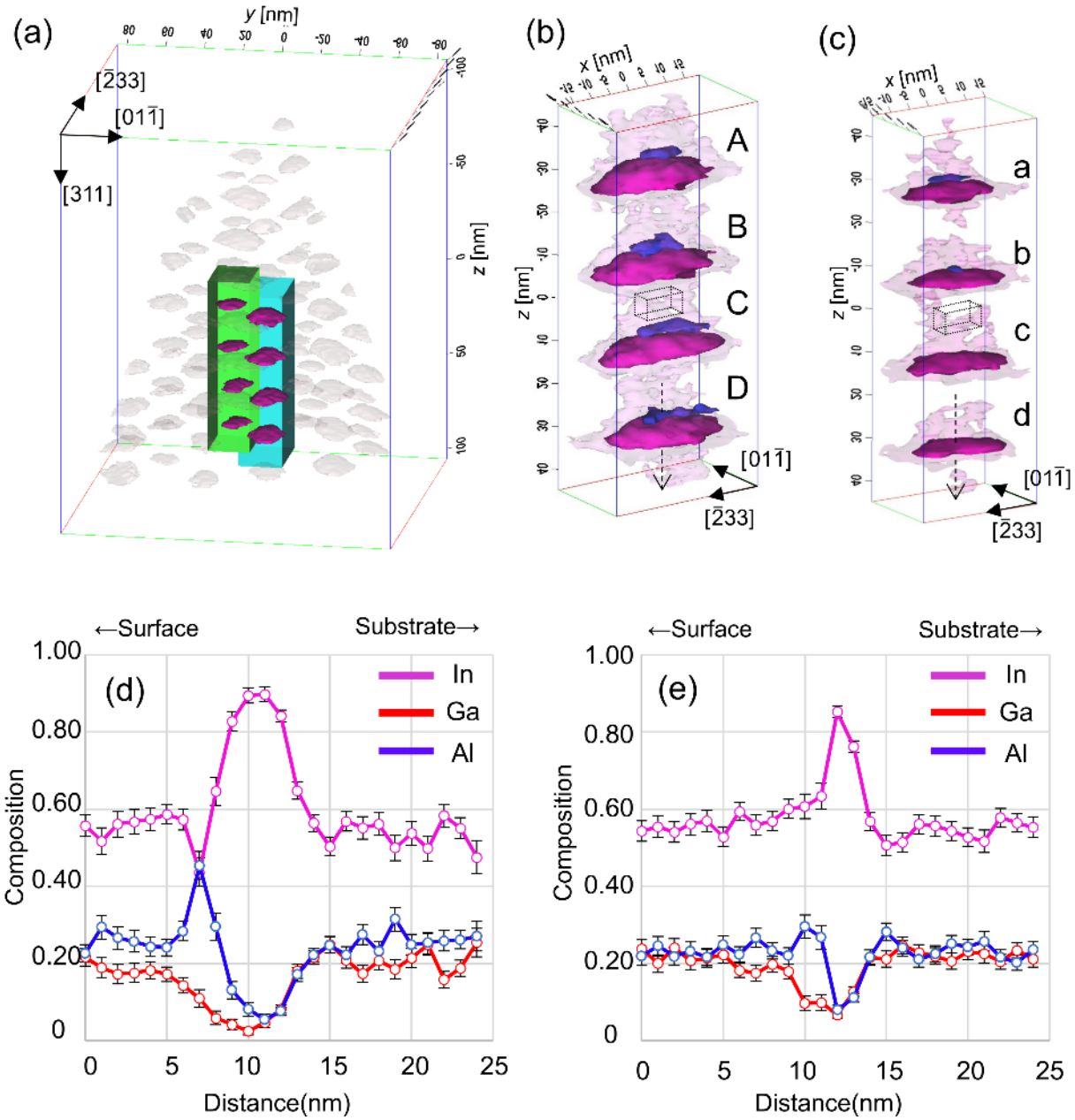

Figure 3. (a) 3D distributions of InAs-QDs obtained from APT. The shape of InAs-QDs is indicated by the iso-concentration surface with the 70% In composition. QD columns containing QDs with in-plane sizes of approximately (b) 32 nm × 20 nm extracted from the blue-framed region and (c) 24 nm × 16 nm extracted from the green-framed region are shown in (a). The iso-concentration surfaces of 33% Al, 57% In, and 70% In are indicated in blue, translucent pink, and

pink, respectively. (d) Compositional profiles of In, Ga, and Al along the dashed arrows in (b) and those (e) along the dashed arrows in (c).

Figure 3(b) shows AlAs-rich regions directly above the QDs and columnar-like InAs-rich regions that include the QD columns. Further, AlAs-rich and InAs-rich regions are observed even with small QDs (Figure 3(c)); however, these atomic-scale segregations are weak and absent in some QDs. In compositions calculated from the dashed frames (5 nm × 10 nm× 10 nm) in Figures 3(b) and 3(c) are 57.1% and 54.1%, respectively, indicating that columns with smaller QDs have lower In compositions. In compositions of both QD columns were almost 10% higher than the 44.5% spacer layer in the outer region of InAs-QD columns. Figures 3(d) and 3(e) indicate the In, Ga, and Al compositional profiles[29] obtained along the dashed arrows shown in Figures 3(b) and 3(c), respectively. Compositional profiles were plotted for a 5 nm × 5 nm region in the crystal growth plane and separated by 1-nm steps. The region of maximum In composition corresponds to the position of InAs-QDs. Figure 3(d) shows an AlAs-rich region on the surface side of the QD and the reduced In composition in this region. In contrast, no such region is observed in Figure 3(e). These results suggest that the dark contrasts in the HAADF-STEM images in Figures 1(b) and 1(f) correspond to the AlAs-rich region; the compressive strain in Figure 2(b) is caused by the lower In composition in the AlAs-rich region. Further, the stripe-like bright contrast in the HAADF-STEM image in Figure 1(a) and stripe-like lattice expansion region in Figure 2(c) correspond to the InAs-rich region. The structural parameters of QDs such as shape, composition, and strain exhibited a strong correlation. Further, atomic-scale segregations were revealed by STEM with energy-dispersive X-ray spectroscopy (EDS) (Figure S2). The profiles in Figures 3(d) and 3(e) show that Ga and Al were present at the center of InAs-QDs and were more significant in QD-d than in QD-D because of interdiffusion through the interface between the QDs and the

spacer layer.[30, 31] The centers of smaller QDs are closer to the interface, and the ratio of the surface area per volume is relatively larger, i.e., the effect of diffusion is expected to be relatively large.

Next, we considered the formation mechanism of atomic-scale segregations around QDs such as the InAs-rich and AlAs-rich regions. The local surface chemical potential, which determines the migration above the QD, was dominated by the local strain and surface curvature.[32] Figure 4 describes the expected formation mechanism of atomic-scale segregation. Figure 4 shows that the lattice expansion in the crystal growth plane caused by the InAs-QD formation attracted InAs with large lattice sizes during the deposition of the InGaAlAs spacer layer, which resulted in the formation of columnar-like InAs-rich regions. Moreover, lattice expansion in the crystal growth plane promoted the formation of InAs wetting layers and InAs-QDs, leading to the vertical alignment of QDs.[33] The weaker In segregation in smaller QD columns can be attributed to the smaller internal In composition and lattice expansion with a decrease in the QD size. In contrast, GaAs and AlAs with smaller lattices cannot remain above the QDs. Therefore, the formation of columnar-like InAs-rich regions can be explained in terms of the strain, but not the formation of AlAs-rich regions at the apex of the QDs.

The AlAs-rich region near the QD apex was also revealed by APT and scanning tunneling microscopy characterization of GaAs-QD embedded in an AlGaAs layer.[24] They reported that the convex shape of the QDs induces migration of atoms from the QD apex to the sides, leaving Al with a short diffusion length near the apex to form AlAs-rich regions. Based on this background, we discuss the AlAs-rich region near the apex of the InAs-QD embedded in the InGaAlAs examined herein. In, Ga, and Al atoms are not stable at the apex of the QD, which exhibits the largest surface curvature during the deposition of InGaAlAs spacer layers. This is attributed to the local surface chemical potential increasing near the apex of the QD, which exhibits the largest

surface curvature, facilitating migration.[33] The cohesive energy increases in the order of InAs, GaAs, and AlAs,[34] and the formation of AlAs with the highest cohesive energy is preferred on the epi-surface. Hence, the diffusion length on the epi-surface decreases in the order of In, Ga, and Al. The diffusion length of the Ga atom is ~0.7 μm on a GaAs substrate at 550 °C, while that of an Al atom is ~0.02 μm, which is smaller by more than one order of magnitude.[35] Therefore, In and Ga atoms preferentially leave the QD apex, leaving Al atoms behind. AlAs segregation is weak in smaller QDs because the surface curvature near the apex decreases with decreasing QD size. Figure 4 illustrates that the contribution of surface curvature exceeds that of strain only in the apex region with the largest surface curvature, resulting in AlAs segregation. By contrast, the effect of strain becomes more dominant in regions except for the apex where the surface curvature is small, thereby suppressing AlAs segregation and leading to InAs segregation.

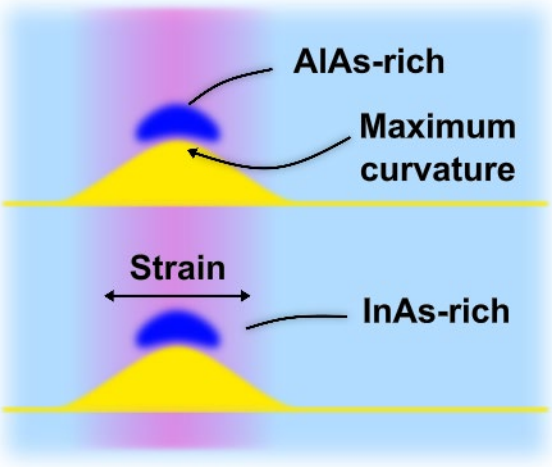

Figure 4. Schematic of the expected mechanism of atomic-scale segregation around the QDs. Yellow and light-blue regions show the InAs-QD and InGaAlAs spacer layers, respectively, whereas violet and blue regions indicate the InAs-rich and AlAs-rich regions, respectively, in the InGaAlAs spacer layer.

Two-dimensional (2D) In, Ga, and Al composition maps[29] inside QD-D are shown in Figures 5(a)–(c), respectively. The interior of the QD-D was extracted at 11 nm × 11 nm in the crystal growth plane and 2 nm in the crystal growth direction, and then, they were projected in the crystal growth direction. The extracted areas are shown in Figure S3. Figures 5(d)–(f) present scatter plots that show the correlation between In and Al, In and Ga, and Ga and Al compositions in these 2D composition maps, respectively. The correlation coefficient *r* for each distribution is indicated in the figures; these results suggest strong negative correlations between the In and Al and In and Ga compositions and the weak positive correlations between the Ga and Al compositions in the QD. The strong negative correlation between the distribution of In and Al atoms, and that of In and Ga atoms can be attributed to the immiscibility of InAs and AlAs and that of InAs and GaAs caused by the large difference in lattice constants.[36] Conversely, the weak positive correlation between the Al and Ga atom distributions could be attributed to the relatively high miscibility of AlAs and GaAs because their lattice constants are almost the same.[36] The immiscibility between InAs and AlAs can accelerate the Al segregation and In reduction in the AlAs-rich region shown in Figure 3(d).

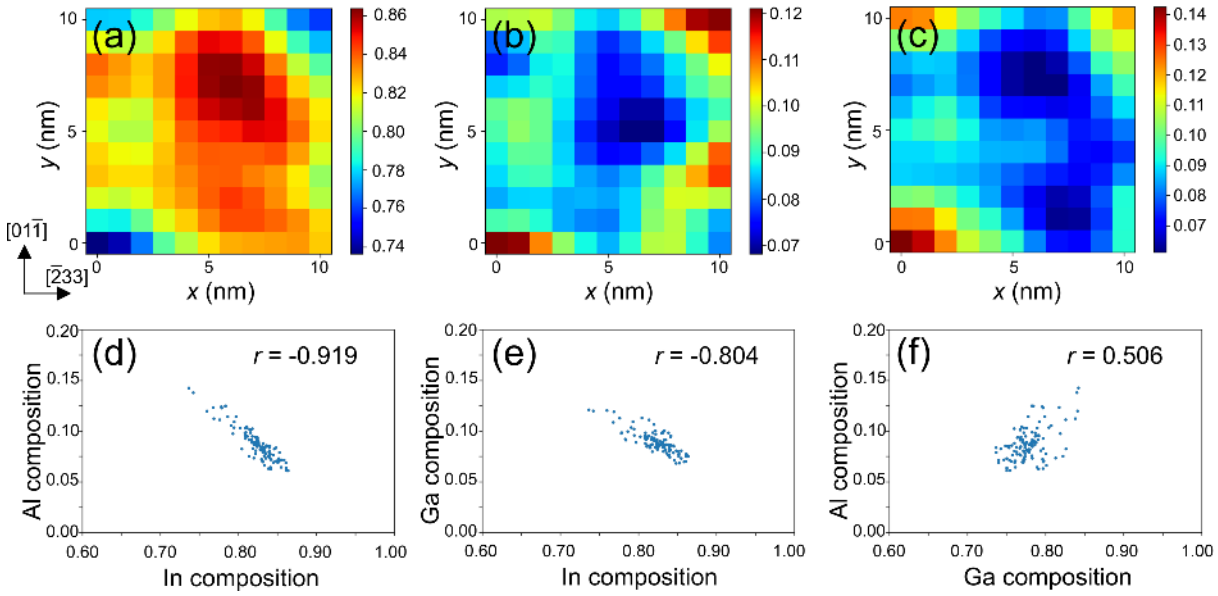

Figure 5. 2D composition map of (a) In, (b) Ga, and (c) Al in the crystal growth plane inside QD-D. Scatterplots indicating the correlation between (d) In and Al, (e) In and Ga, and (f) Ga and Al compositions in the 2D composition maps with the correlation coefficient *r*.

To conclude, we performed atomic-scale multimodal characterization on self-assembled InAs-QDs with InGaAlAs spacer layers on InP substrates using APT, STEM, and GPA to comprehensively understand their complexly correlated structural parameters. We observed characteristic atomic segregation, such as columnar-like InAs-rich regions including QD columns and AlAs-rich regions at the QD apex, which can be explained by the relationship between the effect of local strain and surface curvature. Furthermore, the distribution of group-III atoms inside the QDs showed a clear correlation, which could be related to the atomic segregation. In the future, we will clarify the influence of these atomic segregations on the electronic state of QDs by using density functional theory calculations.

Methods

Preparation of InAs/InGaAlAs QDs. The sample characterized in this study was deposited through molecular beam epitaxy. First, a 100-nm InP buffer layer was deposited on an InP(311)B substrate. Next, a 23-nm $In_xGa_yAl_{1-x-y}As$ (x = 0.512, y = 0.212) layer and a 3.5 atomic layer of InAs wetting layer were deposited. The InAs wetting layer formed QDs via the SK-mode growth. Finally, a superlattice layer comprising InAs-QDs and InGaAlAs spacer layers was deposited over 20 cycles. The topmost InAs-QDs were exposed on the surface. The growth temperature of each layer was 470 °C.

Preparation of thin film specimens for STEM. Thin film specimens were prepared for the plan-view and cross-sectional STEM observation through focused ion beam scanning electron microscopy (FIB-SEM, Helios G4UX, ThermoFisher). The thin film specimens for plan-view observation were processed using a 30 kV Ga ion beam, following which Ar-ion milling was performed at 350 V using a TECHNOORG-Linda Gentle Mill to reduce the Ga ion beam damage. The thickness of the specimen in the [311] direction (direction of electron beam transmission) was approximately 80 nm. Thin film specimens for cross-sectional observation were processed via low-temperature FIB to improve the accuracy of the GPA strain characterization. Group III arsenic crystals can easily form thermal damage layers,[37] which can degrade the STEM image quality and strain characterization accuracy. A 40-nm-thick thin film specimen in the $[\bar{2}33]$ direction (electron beam transmission direction) was processed by reducing the stage temperature to –140 °C to avoid this issue; finally, it was cleaned with a 2 kV Ga ion beam. HAADF-STEM characterization was performed using JEOL ARM-300F. The acceleration voltage was set to 300 kV and the acquisition angle of the HAADF detector was 45–180 mrad.

Preparation of needle-shaped specimen for APT. A needle-shaped specimen for APT was prepared using FIB-SEM based on the general lift-out method.[38, 39] Specimens with a diameter of ~100 nm was processed by annular FIB milling and cleaned with a 500 V Ga ion beam for removing the damage caused by the high-energy Ga ion beam. APT measurements were performed using a local electrode atom probe (LEAP5000XS, AMETEK) under 250 kHz pulsed ultraviolet laser excitation (355 nm) at a specimen temperature of 30 K under ultrahigh vacuum; a laser pulse energy of 100 fJ was selected. For visualization and analysis, IVAS (version 3.8.16) was used to produce 3D atom maps of the specimen.

ASSOCIATED CONTENT

Supporting Information: HAADF-STEM image and intensity profile illustrating the presence of stripe-like bright contrast, composition maps of QDs obtained from STEM-EDS, and extracted area of the 2D composition map inside the QD.

REFERENCES

(1) Huang, X.; Stintz, A.; Hains, C. P.; Liu, G. T.; Cheng, J.; Malloy, K. J. very low threshold current density room temperature continuous-wave lasing from a single-layer InAs quantum-dot laser. *IEEE Photonics Technol. Lett.* **2000**, *12*, 227-229.

(2) Nishi, K.; Yamada, M.; Anan, T.; Gomyo, A.; Sugou, S. long-wavelength lasing from InAs self-assembled quantum dots on (311)B InP by gas-source molecular beam epitaxy. *Proc. Tenth Int. Conf. Indium Phosphide Related Mater.*, Tsukuba, 11–15 May 1998.

(3) Saito, H.; Nishi, K.; Sugou, S. ground-state lasing at room temperature in long-wavelength InAs quantum-dot lasers on InP(311)B substrates. *Appl. Phys. Lett.* **2001**, *78*, 267-269.

(4) Okada, Y.; Oshima, R.; Takata, A. characteristics of InAs/GaNAs strain-compensated quantum dot solar cell. *J. Appl. Phys.* **2009**, *106*, 024306.

(5) Oshima, R.; Takata, A.; Okada, Y. strain-compensated InAs/GaNAs quantum dots for use in high-efficiency solar cells. *Appl. Phys. Lett.* **2008**, *93*, 083111.

(6) Stangl, J.; Holý, V.; Bauer, G. structural properties of self-organized semiconductor nanostructures. *Rev. Mod. Phys.* **2004**, *76*, 725-783.

(7) Roh, C. H.; Park, Y. J.; Kim, K. M.; Park, Y. M.; Kim, E. K.; Shim, K. B. defect generation in multi-stacked InAs quantum dot/GaAs structures. *J. Cryst. Growth*. **2001**, *226*, 1-7.

(8) Shiramine, K.; Horisaki, Y.; Suzuki, D.; Itoh, S.; Ebiko, Y.; Muto, S.; Nakata, Y.; Yokoyama, N. threading dislocations in multilayer structure of InAs self-assembled quantum dots. *Jpn. J. Appl. Phys.* **1998**, *37*, 5493.

(9) Kim, K. M.; Park, Y. J.; Roh, C. H.; Park, Y. M.; Kim, E. K.; Hyon, C. K.; Park, J. H.; Kim, T. W. shape and interband transition behavior of InAs quantum dots dependent on number of stacking cycles. *Jpn. J. Appl. Phys.* **2003**, *42*, 54-57.

(10) Hubbard, S. M.; Cress, C. D.; Bailey, C. G.; Raffaelle, R. P.; Bailey, S. G.; Wilt, D. M. effect of strain compensation on quantum dot enhanced GaAs solar Cells. *Appl. Phys. Lett.* **2008**, *92*, 123512.

(11) Sayari, A.; Ezzidini, M.; Azeza, B.; Rekaya, S.; Shalaan, E.; Yaghmour, S. J.; Al-Ghamdi, A. A.; Sfaxi, L.; M'ghaieth, R.; Maaref, H. improvement of performance of GaAs solar cells by inserting self-organized InAs/InGaAs quantum dot superlattices. *Sol. Energy Mater. Sol. Cells*. **2013**, *113*, 1-6.

(12) Akahane, K.; Ohtani, N.; Okada, Y.; Kawabe, M. Fabrication of ultra-high density InAs-stacked quantum dots by strain-controlled growth on InP(3 1 1)B substrate, *J. Cryst. Growth*. **2002**, *245*, 31-36.

(13) Akahane, K.; Yamamoto, N.; Kawanishi, T. fabrication of ultra-high-density InAs quantum dots using the strain-compensation technique. *Phys. Status Solidi (A)*. **2011**, *208*, 425-428.

(14) Akahane, K.; Yamamoto, N.; Ohtani, N.; Okada, Y.; Kawabe, M. role of Al in spacer layer on the formation of stacked InAs quantum dot structures on InP(3 1 1)B, *J. Cryst. Growth*. **2003**, *256*, 7-11.

(15) Arakawa, Y.; Sakaki, H. multidimensional quantum well laser and temperature dependence of its threshold current. *Appl. Phys. Lett.* **1982**, *40*, 939-941.

(16) Dekel, E.; Gershoni, D.; Ehrenfreund, E.; Spektor, D.; Garcia, J. M.; Petroff, P. M. multiexciton spectroscopy of a single self-assembled quantum dot. *Phys. Rev. Lett.* **1998**, *80*, 4991-4994.

(17) Lee, J.-S.; Ren, H.-W.; Sugou, S.; Masumoto, Y. $In_{0.5}Ga_{0.5}As$ quantum dot intermixing and evaporation in GaAs capping layer growth. *J. Appl. Phys.* **1998**, *84*, 6686-6688.

(18) Wojs, A.; Hawrylak, P.; Fafard, S.; Jacak, L. electronic structure and magneto-optics of self-assembled quantum dots. *Phys. Rev. B.* **1996**, *54*, 5604-5608.

(19) Mo, Q. W.; Fan, T. W.; Gong, Q.; Wu, J.; Wang, Z. G.; Bai, Y. Q. effects of annealing on self-organized InAs quantum islands on GaAs(100). *Appl. Phys. Lett.* **1998**, *73*, 3518-3520.

(20) Hasan, S.; Han, H.; Korytov, M.; Pantouvaki, M.; Campenhout, V. J.; Merckling, C.; Vandervorst, W. InAlGaAs encapsulation of MOVPE-grown InAs quantum dots on InP (001) substrate. *J. Cryst. Growth* **2020**, *531*, 125342.

(21) Vullum, P. E.; Nord, M.; Vatanparast, M.; Thomassen, S. F.; Boothroyd, C.; Holmestad, R.; Fimland, B. O.; Reenaas, T. W. quantitative strain analysis of InAs/GaAs quantum dot. *Mater. Sci. Rep.* **2017**, *7*, 45376.

(22) Cherkashin, N.; Reboh, S.; Hÿtch, M. J.; Claverie, A.; Preobrazhenskii, V. V.; Putyato, M. A.; Semyagin, B. R.; Chaldyshev, V. V. determination of stress, strain, and elemental distribution within In(Ga)As quantum dots embedded in GaAs using Advanced transmission electron microscopy. *Appl. Phys. Lett.* **2013**, *102*, 173115.

(23) Sokolov, P. S.; Petrov, M. Y.; Mehrtens, T.; Müller-Caspary, K.; Rosenauer, A.; Reuter, D.; Wieck, A. D. reconstruction of nuclear quadrupole interaction in (In,Ga)As/GaAs quantum dots observed by transmission electron microscopy. *Phys. Rev. B*. **2016**, *93*, 045301.

(24) Bocquel, J.; Giddings, A. D.; Mano, T.; Prosa, T. J.; Larson, D. J.; Koenraad, P. M. composition profiling of GaAs/AlGaAs quantum dots grown by droplet epitaxy. *Appl. Phys. Lett.* **2014**, *105*, 153102.

(25) Giddings, A. D.; Keizer, J. G.; Hara, M.; Hamhuis, G. J.; Yuasa, H.; Fukuzawa, H.; Koenraad, P. M. composition profiling of InAs quantum dots and wetting layers by atom probe tomography and cross-sectional scanning tunneling microscopy. *Phys. Rev. B*. **2011**, *83*, 205308.

(26) Müller, M.; Cerezo, A.; Smith, G. D. W.; Chang, L.; Gerstl, S. S. A. atomic scale characterization of buried InxGa1-xAs quantum dots using pulsed laser atom probe tomography. *Appl. Phys. Lett.* **2008**, *92*, 233115.

(27) Çelebi, C.; Ulloa, J. M.; Koenraad, P. M.; Simon, A.; Letoublon, A.; Bertru, N. capping of InAs quantum dots grown on (311)B InP studied by cross-sectional scanning tunneling microscopy. *Appl. Phys. Lett.* **2006**, *89*, 023119.

(28) Hÿtch, M. J.; Snoeck, E.; Kilaas, R. quantitative measurement of displacement and strain fields from HREM micrographs. *Ultramicroscopy* **1998**, *74*, 131-146.

(29) Miller, M. K. atom probe tomography, Springer, New York, 2000.

(30) García, J. M.; Medeiros-Ribeiro, G.; Schmidt, K.; Ngo, T.; Feng, J. L.; Lorke, A.; Kotthaus, J.; Petroff, P. M. intermixing and shape changes during the formation of InAs self-assembled quantum dots. *Appl. Phys. Lett.* **1997**, *71*, 2014-2016.

(31) Akahane, K.; Matsumoto, A.; Umezawa, T.; Yamamoto, N. fabrication of In(P)As quantum dots by interdiffusion of P and As on InP(311)B substrate. *Crystals.* **2020**, *10*, 90.

(32) Xie, Q.; Chen, P.; Madhukar, A. InAs island-induced-strain driven adatom migration during GaAs overlayer growth. *Appl. Phys. Lett.* **1994**, *65*, 2051-2053.

(33) Xie, Q.; Madhukar, A.; Chen, P.; Kobayashi, N. P. vertically self-organized InAs quantum box islands on GaAs(100). *Phys. Rev. Lett.* **1995**, *75*, 2542-2545.

(34) Liu, W.; Zheng, W. T.; Jiang, Q. first-principles study of the surface energy and work Function of III-V semiconductor compounds. *Phys. Rev. B.* **2007**, *75*, 235322.

(35) Koshiba, S.; Nakamura, Y.; Tsuchiya, M.; Noge, H.; Kano, H.; Nagamune, Y.; Noda, T.; Sakaki, H. surface diffusion processes in molecular beam epitaxial growth of GaAs and AlAs as studied on GaAs (001)-(111)B facet structures. *J. Appl. Phys.* **1994**, *76*, 4138-4144.

(36) Stringfellow, G. B. miscibility gaps and spinodal decomposition in III/V quaternary alloys of the type $A_xB_yC_{1-x-y}D$. *J. Appl. Phys.* **1983**, *54*, 404-409.

(37) Qi, H.; Wang, Q.; Li, Y.; Zhang, X.; Liu, Z.; Wang, Y.; Zhang, S.; Xia, W.; Jin, G. thermal process and surface damage of GaAs induced by 532 nm continuous laser. *Appl. Surf. Sci.* **2007**, *254*, 1373-1376.

(38) Miller, M. K.; Russell, K. F.; Thompson, G. B. strategies for fabricating atom probe specimens with a dual beam FIB. *Ultramicroscopy* **2005**, *102*, 287-298.

(39) Thompson, K.; Lawrence, D.; Larson, D. J.; Olson, J. D.; Kelly, T. F.; Gorman, B. in situ site-specific specimen preparation for atom probe tomography. *Ultramicroscopy* **2007**, *107*, 131-139.